

SOME PROBLEMS OF LINEAR FILTRATION OF THE IMAGES DISTORTED BY SCATTERING MEDIA

V.V. Belov, B.D. Borisov, and N.V. Molchunov

*Institute of Atmospheric Optics,
Siberian Branch of the Academy of Sciences of the USSR, Tomsk
Received April 1, 1991*

The possibility of using the linear filters in the problem of restoration of the images distorted by the optically dense scattering formations of the atmosphere has been investigated. Using a spatially bounded object as an example it has been shown that for real digitized images, which incorporates a noise component, an application of smoothing of the solution is required in order to compensate for the quality losses caused by noise, errors in specifying the pulse transfer function of the distorting medium, and spatial boundedness associated with the formation of the image frame.

The effectiveness of airborne sounding of the Earth's surface is limited by scattering layers such as clouds, hazes, and fogs which distort the detected image in a specific way and thereby make the image processing, which is carried out with the purpose of monitoring the state of the natural medium and the objects of artificial origin, more difficult. In this connection as the sounding systems are developed and the classes of the sounded objects are extended, a need for studying and developing the methods, which are capable of restoring the images distorted by such formations, increases.

This paper is devoted to studying the possibility of using the well-known methods, which have already become classic, for restoration of the images distorted by the scattering media. In so doing, considerable attention is devoted to the analysis of sources of the errors which arise in the process of restoration of the digitized images on a computer.

Let us consider some details of the image formation at the output from the recording device with an account of the transfer of an incoherent optical signal through turbid media.

The effect of such a medium on the process of image formation is analogous to that of the low-frequency spatial filter, whose output signal is described by the convolution integral equation

$$g_a(x, y) = \int_{-\infty}^{\infty} \int_{-\infty}^{\infty} f(\xi, \eta) h(x - \xi, y - \eta) d\xi d\eta = f(x, y) * h_a(x, y), \quad (1)$$

where $h_a(x, y)$ is the pulse response function of the medium (the point spread function (PSF)), $f(x, y)$ is the initial signal from the object, and $g_a(x, y)$ is the image formed at the detector input.

The recording device in the process of forming the image can be regarded as one more low-frequency spatial filter with the pulse response function $h_n(x, y)$, which also reduces the dynamic range of the initial signal and contributes to the noise component $n(x, y)$. The total pulse response function of the transmitting-recording channel is represented by a convolution of the pulse response functions of its components, i.e.,

$$h(x, y) = h_a(x, y) * h_n(x, y). \quad (2)$$

The recorded image signal can be now described in the following way:

$$g_d(x, y) = D[f(x, y) * h(x, y) + n(x, y)], \quad (3)$$

where D is the operator of reduction of the dynamic range. In particular, its function can be carried out by a photodetector within the linear portion of the frequency response as well as by an analog-to-digital converter (ADC) with the fixed number of bits; for this reason, the action of the operator D is extended also to the noise $n(x, y)$ introduced by the recording device. Any optical device bounds spatially the recorded image, i.e., forms a frame. As a rule, a rectangle is such a bounded area. In the case of digital images it is more convenient to use the square frames (or rasters), since the mathematical apparatus of discrete integral transformations is well adapted to them.

Thus, the image at the output from the recording device can be represented in the form

$$g(x, y) = D\{R[f(x, y) * h(x, y) + n(x, y)]\}, \quad (4)$$

where R is the operator of frame formation, which has no effect on the noise properties.

Note that, when carrying out the restoration, the frame formation may be an extremely unfavorable factor, significantly affecting the restoration quality. Let us assume that the frame formation results in a truncation of the image $f(x, y)$ outside of the intervals $|x| > p$ and $|y| > p$ so that $f(x, y) = 0$ outside of the given intervals. The image truncation is equivalent to its multiplication by the weighting function of the window

$$\omega(x, y) = \begin{cases} 1, & |x| < p \text{ and } |y| < p, \\ 0, & |x| \geq p \text{ and } |y| \geq p. \end{cases}$$

The spectrum of the image obtained after its truncation is equal to a convolution of the spectra of the image and the window, with the spectral function being a two-dimensional sinc function. As a result, parasitic components at higher spatial frequencies, multiple of $2\pi/p$, have arisen in the image spectrum (Gibbs' phenomenon).¹ In connection with the fact that the problem of estimating the image $\hat{f}(x, y)$ from integral equation (1) is ill-posed,⁴ the frame formation can lead to markedly amplified distortions.

If an aerosol-gaseous atmosphere is considered as a scattering medium, then its PSF is wide.² In this connection, note that an analogous growth of the distortions may also give rise to the truncation of the PSF, which is used for the image restoration.

Let a continuous image be digitized with the help of a grid of the Dirac delta-pulses spaced at the interval Δs . We shall assume that the discretization has been made with an interval that allows us to avoid the overlap of the periodically repeated image spectrum. In this case the action of the operator R determines the size of the $N \times N$ square raster at the nodes of which the readings of the distorted image are resided while the action of the operator D virtually reduces to rounding off these readings to the nearest integer on the scale determined by the number of bits of the ADC. As a result, the two-dimensional array of pixels is formed

$$g_{ij} = \sum_{k=1}^N \sum_{l=1}^N f_{kl} h_{i-k, j-l} + n_{ij}. \quad (5)$$

In order to perform an image restoration based on the recorded pixels g_{ij} , we will employ the PSF's calculated according to the technique proposed by V.V. Belov et al. or measured in the laboratory experiments.³ In so doing, on the one hand, the realizations of the PSF will incorporate an error caused by inaccuracy of the calculational methods or the measurement errors; on the other hand, a need for the PSF truncation at some level can arise so that to fit the prescribed size of the raster N . For this reason, a series of numerical experiments was performed on estimating the effect of the following factors on the accuracy of the image restoration:

- inaccuracies in specifying the PSF;
- the quantization range and instrumental noise incorporating the quantization noise;
- the spatial boundedness associated with the formation of the frame.

The investigations were carried out according to the following schemes:

1. Based on the calculated and measured PSF's of the model cloudy media the processes of both the image distortion and restoration were computer simulated.
2. The image was distorted in a laboratory experiment by means of modeling the conditions of observation through the local layer of the turbid medium and was restored with the help of the calculated and measured PSF's.

In both cases the observation model was characterized by the PSF with circular symmetry, in addition, the optical transfer function (OTF), which is a Fourier transform of the PSF, was assumed to be a real function.

In order to minimize the losses associated with the frame formation, the ratio of the size of the raster N and that of the object N_f was chosen from the condition $N/N_f > 10$. In numerical experiments a test object in the form of a uniform circle with the diameter $N_f = 25$ pixels and 250 brightness levels was used. The test object was located at the center of the square raster with 256×256 pixels against a zero background. The noise component was not computer simulated (an image with noise was recorded in the laboratory experiment).

It should be noted that the chosen test object has a virtually infinite spectrum and, therefore, can serve as a good standard when estimating the performance of the restoration algorithms, in particular, their possibility of reconstructing the high spatial frequencies.

The image in the numerical experiment was distorted by means of convolution of the test object and the calculated (by the Monte Carlo method²) or measured³ PSF's in the frequency domain. If necessary, the PSF was interpolated with the required step by the spline approximation method and transformed at the 256×256 grid. In order to eliminate the overlapping effect, the rasters of the object and of the PSF were additionally padded with zeroes to the 512×512 pixels prior to convolution. The frame (action of the operator R) was formed by truncating the result down to the 256×256 pixels. Before recording on a disc, the image pixels were scaled to the required range predetermined by the number of bits of the ADC, and were rounded off to the nearest integer (action of the operator D). For example, for a 5-bit grid the maximum signal amplitude was 30 while for an 8-bit grid it was 250 and for a 10-bit one it amounted to 1020.

In order to obtain a consistent estimate of the results of the numerical and laboratory experiments, in the latter we used a diffuse self-glowing test object shaped as a disk 6 mm in diameter, whose transformation comprised 25 pixels per diameter in the computer memory. Here the spatial quantization step was 0.24 mm/pixel. The test object was recorded by a high-resolution TV camera with compensation for the nonuniformity of the photocathode sensitivity. The scattering medium was prepared by dissolving milk in a distilled water enclosed in a cell with a working diameter of 440 mm. The distance from the test object to the center of the disperse layer l was varied so that we could simulate three types of typical atmospheric optical situations, illustrated in Fig. 1. The figure shows three types of vertical profiles of the extinction coefficients β_{ext} . Figure 1a corresponds to the case in which the underlying surface was covered with the optically dense scattering layer (e.g., fog), figure 1b refers to the case in which the layer was slightly above the surface, and figure 1c illustrates the case when the viewing line intersected cloudiness. Note that the PSF shape and its width are substantially different for the three cases under consideration. If for the first situation the PSF can be approximated by an exponential function, in the last case $h(r) = \delta(r) + \text{const}$, where $\delta(r)$ is the delta function and $r = \sqrt{x^2 + y^2}$.

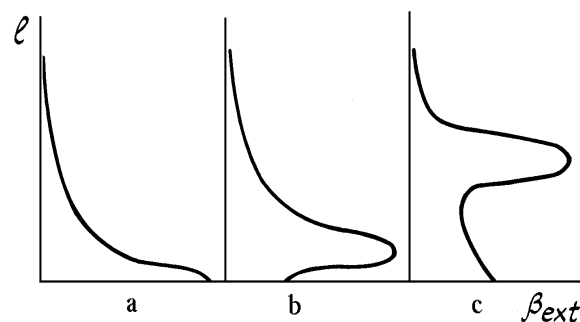


FIG. 1. The vertical profile of the extinction coefficient as a function of the position of the scattering.

The optical thickness τ of the scattering layer was monitored with an individual measuring channel in the experiment. The distorted image was recorded through a layer with $\tau = 7.0$. The reference image of the test object was recorded through a cell filled only with the distilled water.

In order to set the analog TV signal into the computer, a videoprocessor with a high-speed 8-bit ADC was employed. For the purpose of optimal utilization of the ADC bits, the intensity of the light flux from the test object was regulated by neutral light filters positioned in front of the light source; in so doing, the brightness of pixels of the recorded image was in the range 0–250. In order to reduce the noise component, 32 digitized frames were averaged. The image recorded in the byte format was located on the raster with 256×256 pixels.

The distorted images were restored with the use of an inverse filter and Wiener's filter analogous to that used in Refs. 5 and 6, as well as with the use of Tikhonov's regularization technique.⁷ The transfer functions of the filters are given by the formulas in accordance with the above-indicated order.

$$H_i(\omega_x, \omega_y) = \frac{1}{H(\omega_x, \omega_y)}; \tag{6}$$

$$H_W(\omega_x, \omega_y) = \frac{H^*(\omega_x, \omega_y)}{|H(\omega_x, \omega_y)|^2 + A}; \tag{7}$$

$$H_T(\omega_x, \omega_y) = \frac{H^*(\omega_x, \omega_y)}{|H(\omega_x, \omega_y)|^2 + \alpha(\omega_x^2 + \omega_y^2)}, \tag{8}$$

where $H(\omega_x, \omega_y) = F[h(x, y)]$ is the optical transfer function of the scattering layer, F is the symbol of the Fourier transform $|H(\omega_x, \omega_y)|^2 = H(\omega_x, \omega_y) H^*(\omega_x, \omega_y)$, $H^*(\omega_x, \omega_y)$ is the complex conjugate to $H(\omega_x, \omega_y)$. A is the parameter of Wiener's filter, α is the regularization parameter, $\omega_x = \omega_m = m\Delta\omega_x$, $\Delta\omega_x = 2\pi/N$; $\omega_y = \omega_n = n\Delta\omega_y$, $\Delta\omega_y = 2\pi/N$; $m = 1, 2, \dots, N$, and $n = 1, 2, \dots, N$.

In order to estimate the image quality and completeness of the PSF, the criterion of normalized rms error was used:

$$\varepsilon = \frac{\|\varphi_{ij} - \hat{\varphi}_{ij}\|}{\|\varphi_{ij}\|} \cdot 100, \tag{9}$$

where φ_{ij} is the initial test object or the complete PSF and $\hat{\varphi}_{ij}$ is the resulting distorted or restored test object, i.e., the truncated PSF.

In order to numerically estimate the effect of the truncation of the PSF on the restoration accuracy, the distorted images were formed with the help of the PSF's calculated for the three typical positions of the scattering layer with $\tau = 3.75$. In order to cover the energy maximum with the given raster with 256×256 pixels, the PSF was interpolated with larger step being equal to 0.4 mm/pixel. The operators D and R were not involved. The obtained images were characterized by the normalized rms error of 85.4, 91.2, and 96.1% for the first, second, and third positions of the scattering layer, respectively.

In the numerical experiment the PSF width was periodically decreased in the radius at 10 pixels per one iteration. The first iteration was an exception, since a radius was decreased by a single pixel.

The calculated results are listed in Table I for the three positions of the scattering layer. The first column of the table gives the PSF (ε) used in the process of image restoration. The next two columns contain the normalized rms error of restoration with the use of the Wiener's filter when the parameter A was equal to 0.00001 and 0.0001. The last two columns present the normalized rms error of restoration based on Tikhonov's regularization technique with the regularization parameter $\alpha = 1 \cdot 10^{-8}$ and $1 \cdot 10^{-9}$.

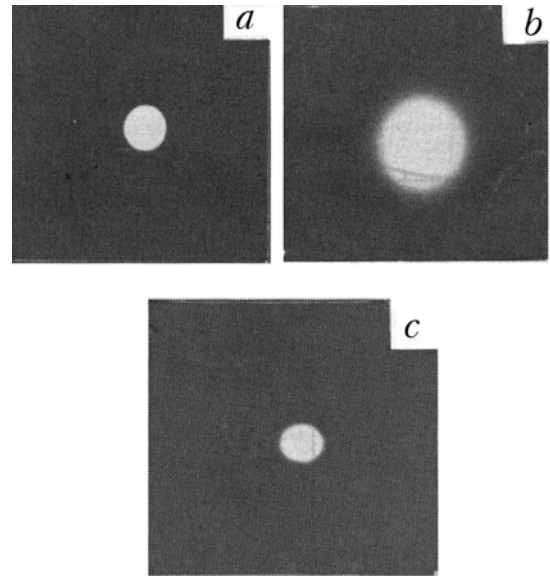


FIG. 2. Images of the test object.

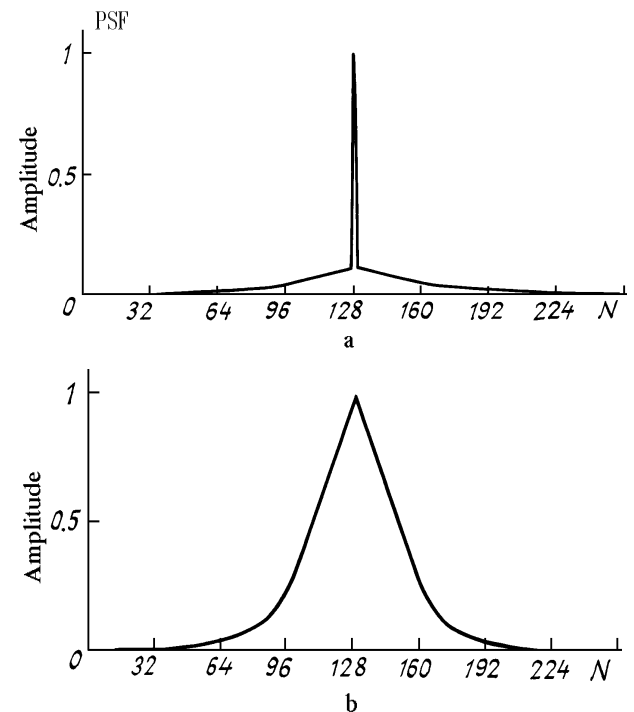


FIG. 3. The PSF profiles.

TABLE I.

Normalized rms error of PCF, %	Normalized rms error of restoration (%)				
	Inverse filter	Wiener's filter		Tikhonov's regularization	
		A=0.00001	A=0.0001	$\alpha=1.0E-8$	$\alpha=1.0E-9$
1	2	3	4	5	6
<i>l</i> = 22 mm					
0.01	0.0	3.6	17.9	19.9	8.0
0.18	0.3	3.6	17.9	19.9	8.0
0.44	0.8	3.8	18.1	19.9	8.1
0.86	1.9	4.5	18.5	20.0	8.4
1.66	4.5	6.6	19.7	20.6	9.6
2.72	8.7	10.4	21.9	21.9	12.3
3.89	13.5	15.0	24.9	24.3	16.3
5.37	19.6	20.8	29.1	28.0	21.6
7.52	27.4	28.3	34.9	33.7	28.9
10.96	38.1	38.7	43.5	42.4	39.1
16.03	51.8	52.2	55.1	54.5	52.4
23.01	68.3	68.3	69.8	69.6	68.6
30.06	80.7	80.8	81.3	81.7	80.8
<i>l</i> = 89 mm					
0.16	17.0	14.0	37.9	26.2	10.9
1.65	898.0	14.7	38.0	26.8	32
3.51	934.4	17.0	38.5	28.8	36.8
5.92	196.8	21.6	39.5	32.8	53.4
9.53	90.8	27.2	42.1	35.8	54.7
12.83	173.4	31.1	45.5	38.2	40.4
15.54	228.0	37.5	49.9	42.6	43.1
18.04	483.3	44.9	53.9	50.4	101.7
20.40	355.4	49.6	58.2	52.8	59.7
22.79	108.4	56.7	63.1	59.0	65.2
25.61	117.0	63.7	68.6	65.8	75.7
31.24	1141.0	98.3	72.4	132.4	404.2
65.01	189.3	98.4	88.7	183.7	286.6
<i>l</i> = 229 mm					
0.12	1.8	19.2	54.3	21.8	7.9
1.15	305.4	24.6	54.1	91.9	239.6
2.32	114.0	37.4	54.5	75.4	106.5
3.73	621.1	49.7	55.4	129.9	405.2
5.76	192.4	55.5	55.7	102.9	174.4
7.73	8426.6	209.5	58.1	1123.7	5145.4
9.54	1103.3	94.2	58.5	298.8	777.5
11.55	146.8	49.1	62.8	83.2	132.9
14.30	194.6	70.1	61.7	127.6	180.9
18.88	171.0	98.5	66.7	146.1	167.9
27.44	128.0	77.1	80.6	91.7	120.6
44.64	117.4	91.5	86.4	96.9	113.1
56.40	195.1	99.1	95.1	97.3	192.4

It follows from the data of Table I that the main portion of the energy of the PSF for the case, which corresponds to Fig. 1a, is concentrated near the central pixel, since radial truncation of the PSF from 127 to 7 pixels results in an increase of the normalized rms error from 0.01 to 30.1%. Truncation of the PSF in this case leads to a smooth growth of the restoration error for all of the filters used. In this case a substantial growth in the restoration error is observed when truncation of the PSF is sufficiently great, i.e., from 128 to 57 pixels or when the normalized rms error is greater than 3%.

A wider PSF with a complicated shape of the wings is typical of the second case (Fig. 1b); as a result, even a

small radial truncation, e.g., down to 117 pixels with an error of 1.65% makes it impossible to use the inverse filter. Although the capacity for work of the filters with the regularizing additions is preserved, the reconstruction quality turns out to be low here.

In order to compensate for the distortions, which arise in the case corresponding to Fig. 1c, the use of the inverse filtration is apparently inadvisable, since even in the case in which the PSF is truncated insignificantly a substantial increase in the restoration error is observed. As follows from the PSF shape and the nature of the distortions, here one can preferably refer to a need for a gradation correction rather than frequency one.

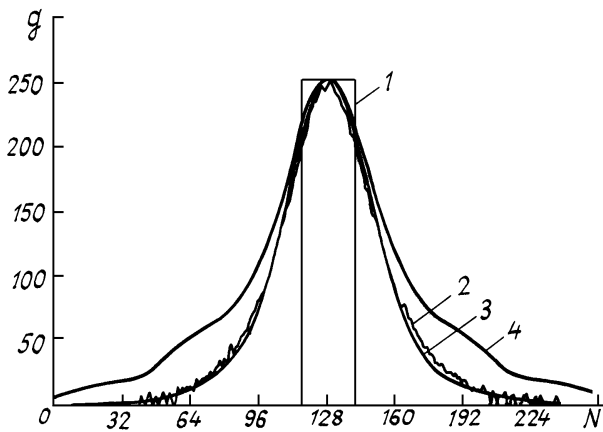


FIG. 4. The image profiles.

Thus, we can conclude that in the process of restoration of the images distorted by the scattering layers with the wide PSF's, a quite high sensitivity of the resulting accuracy to the errors in specifying the PSF wings is observed. The use of the regularization filters makes it possible to obtain the approximate solution, whose error depends on the accuracy of the initial PSF and on the position of the scattering layer on the viewing line. Better results can be obtained for geometric optics situations in which the scattering layer is localized in the first position, i.e., when the PSF is a smooth sufficiently steep decaying function. It is this situation in which we performed the further experiments (Fig. 1a).

The effect of the quantization range and noise (the operator D) as well as of the spatial boundedness (the operator R) associated with the frame formation on the restoration quality has been investigated. In the numerical experiment we used the calculated PSF for a cloudy medium with $\tau = 3.75$ as well as the PSF obtained in the laboratory experiment for the model cloudy medium with $\tau = 7.00$. The spatial quantization step size in both cases was 0.24 mm/pixel.

TABLE II.

The number of bits of the ADC	Normalized rms error of restoration					
	$\tau = 3.75$			$\tau = 7.0$		
	D	R	DR	D	R	DR
5	34.9	23.1	34.9	72.1	61.1	72.1
6	29.2	23.1	29.2	64.3	61.1	64.3
8	24.0	23.1	24.0	61.2	61.1	61.2
10	23.3	23.1	23.3	61.2	61.1	61.2

The results of numerical experiment with Wiener's filter (the parameter $A = 0.00015$) are presented in Table II. In order to obtain the consistent estimates, the normalized rms errors were calculated after scaling the restored image on the range of the 8-bit ADC and recording them in the byte format on a magnetic disk. The distorted images were characterized by the normalized rms errors of 65.7 and 150.6% for $\tau = 3.75$ and 7.0, respectively.

It follows from our results that

a) even in the case in which the PSF is exactly known and external noise sources are absent an uncertainty has arisen due to the finite representation of the number at the output from the ADC (the quantization noise) that leads to a significant error in the solution,

b) extension of the digital grid of the ADC weakly affects the restored image,

c) the frame formation gives rise to the growth of the restoration error also when the object has small size, for which the amplitude of the signal carried out of the frame by the PSF wings constitutes a small value, which lies below the sensitivity threshold of the ADC.

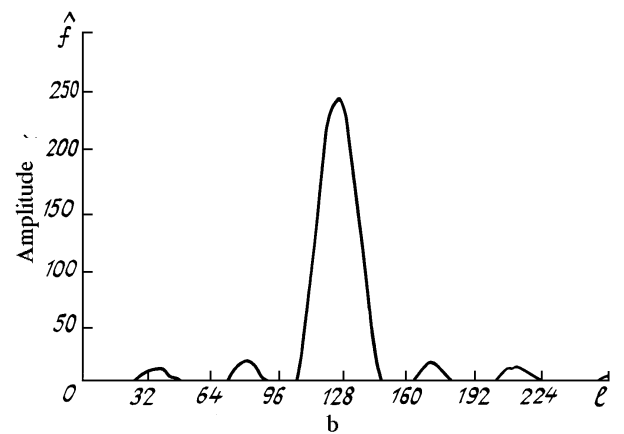
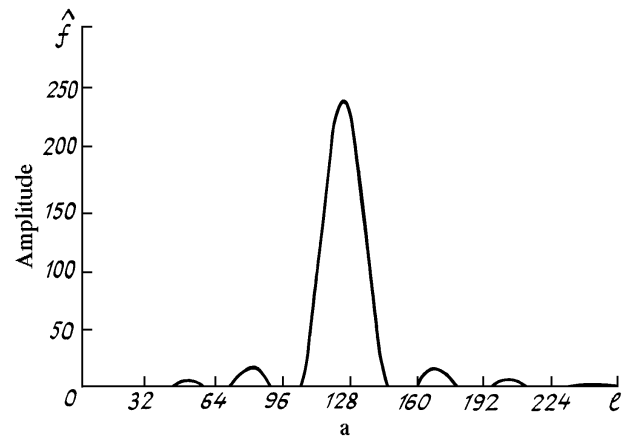


FIG. 5. The profiles of the image restored based on Tikhonov's regularization method.

Let us consider the resulting restored images, which have been obtained in the laboratory experiment. Figure 2 shows the images of the object (a) and its distortion (b), which is characterized by a large value of the normalized rms error equal to 159.7%. The profiles of the calculated (for a medium with $\tau = 7.6$) PSF and the measured one (for a medium with $\tau = 7.0$), respectively, are shown in Figs. 3a and b. Figure 4 shows the profiles of the model object (curve 1), of the image distorted in the laboratory experiment (curve 2), and of the results of distortion of the model object with the help of the measured PSF (curve 3) and the calculated one (curve 4). As one can see, the measured PSF adequately reflects the process of distortion formation, the error within the limits of the 256x256 raster does not exceed 15%. At the same time, the calculated PSF incorporates a rather large error and, as a consequence, the normalized rms error of the model distorted image in comparison with the recorded image amounts to 63.5% (on the 256x256 raster). It looks as though with the help of the measured PSF we can obtain a higher quality restoration; however, this does not take place, because there is a need for smoothing (in order to control the noise,

the truncation of the image frames and of the PSF) by means of regularization of the restoration algorithm. As a result, the use of the calculated and measured PSF's yields an identical results in practice.

Figure 2c shows the resulting restoration of the distorted image, which was recorded in the laboratory experiment (Fig. 2b). The reconstruction based on Tikhonov's regularization method with the measured PSF was employed. The choice of the optimal value of the regularization parameter α_{opt} was made by way of calculating the set of

regularized solutions $\hat{f}_{ij}^{\alpha_k}$, for which the normalized rms error was calculated in accordance with Eq. (9). A value of α_k , for

which $\varepsilon_k(\hat{f}_{ij}^{\alpha_k})$ reaches the minimum, was chosen as optimal.

As a result, it was found that $\alpha_{\text{opt}} = 1.0 \cdot 10^{-7}$. Using it we have obtained a smoothed solution with the normalized rms error $\varepsilon_{\text{opt}} = 43.6\%$. The profile of this image is shown in Fig. 5a, while the profile of the image obtained by means of the same filter but with the calculated PSF, is shown in Fig. 5b. As one can see, they differ only in the region of overshoots, for which Gibb's phenomena are responsible. When $\alpha = 0.1\alpha_{\text{opt}}$ significant increase of noise is observed, while at $\alpha = 10\alpha_{\text{opt}}$ still stronger smoothing occurs. The value of the normalized rms error for the first case is 48.8% and for the second case it is 58.4%.

Thus, the distortions of the images recorded under the conditions of atmospheric-optics situation of the first type (when the scattering layer with a moderate optical density is located near the object) is characterized by the large normalized rms error. In this case, the use of the linear filters makes it impossible to compensate for the losses of the high spatial frequencies. In the considered situation we have succeeded but in restoration of the average diameter of the object measured at half-maximum of the amplitude.

REFERENCES

1. W. Pratt, *Digital Image Processing* (John Wiley & Sons, New York, 1978).
2. V.V. Belov, B.D. Borisov, and I.Yu. Makushkina, *Opt. Atm.* **1**, No. 2, 18 (1988).
3. B.D. Borisov, *Opt. Atm.* **1**, No. 6, 29 (1988).
4. M. Bertero, T.A. Podzho, and V. Torre, *Proc. IEEE* **76**, No. 8, 17-40 (1988).
5. L.R. Beriel and J. Bescos, *Appl. Opt.* **22**, No. 18, 2772-2780 (1983).
6. R.H.T. Bates and M.J. McDonnell, *Image Restoration and Reconstruction* (Clarendon Press, Oxford, 1986).
7. A.N. Tikhonov, A.V. Goncharkii, V.V. Stepanov, and A.G. Yagola, *Numerical Methods for Solving Ill-posed Problems* (Nauka, Moscow, 1990).